Closed loop adaptive optics with a laser guide star for biological light microscopy

Saunter, Christopher, Bourgenot, Cyril, Girkin, John, Love, Gordon

Christopher D. Saunter, Cyril Bourgenot, John M. Girkin, Gordon D. Love, "Closed loop adaptive optics with a laser guide star for biological light microscopy," Proc. SPIE 8253, MEMS Adaptive Optics VI, 82530J (15 February 2012); doi: 10.1117/12.909927

SPIE.

Event: SPIE MOEMS-MEMS, 2012, San Francisco, California, United States

Closed Loop Adaptive Optics with a Laser Guide Star for Biological Light Microscopy

Christopher D. Saunter[a], Cyril Bourgenot[a], John M. Girkin[a] and Gordon D. Love[a]

[a]Department of Physics and Biophysical Sciences Institute, Durham University, Durham, DH13LE, United Kingdom

ABSTRACT

We report on the development of a widefield microscope that achieves adaptive optics correction through the use of a wavefront sensor observing an artificial laser guide star induced within the sample. By generating this guide star at arbitrary positions and depths within the sample we allow the delivery of high-resolution images. This approach delivers much faster AO correction than image optimization techniques, and allows the use of AO with fluorescent imaging modalities without generating excessive photo-toxic damage in the sample, or inducing significant photo-bleaching in the flurophore molecules.

Keywords: Adaptive Optics, Microscopy, Fluorescence, Image Optimization, Guide Star

1. INTRODUCTION

Adaptive optics (AO) was first developed for imaging through atmospheric turbulence where light for a wavefront sensor (WFS) is gathered from either a natural or a laser guide star. There has been much recent interest in applying these techniques to microscopy so aberrations in both the specimen and the optic train can be corrected [1,2]. Most work on microscope AO has involved image optimization techniques, sometimes referred to as wavefront senseless AO [3-5]. The fluorescent processes used to generate these images in epi-fluorescence and confocal microscopy suffer from various detrimental effects. In photobleaching, the excitation fluorescence light ultimately destroys the fluorophore molecule. The excitation light also generates triplet states amongst both the flurophores and intrinsic chromaphores in the sample [6] which leads to both the loss of the flurophore and also free radicals and other toxic compounds. Whilst image optimization techniques work well, they require many images to implicitly measure one wavefront leading to the accumulation of significant photon related damage in the sample. The time-sequential nature also renders them unsuitable for dynamic samples, and prone to the detrimental effects from the fluorescence process. The requirement for many images is particularly onerous when used with a beam scanned system such as confocal or multi-photon microscopy.

Motivated by these challenges, recent work has been published on closed loop AO that uses a spatially resolved WFS [7-11] to rapidly and accurately determine wavefront errors prior to correction. A major challenge for AO microscopy is obtaining a good signal for measurement by the WFS. One approach is to use a fluorescent bead within the sample [7,9] to provide a localized point-like source, This type of closed loop AO is analogous to natural guide star AO – in that if the object of interest is close to the bead (axially as well as transversely, with microscopy being 3 dimensional) then the WFS will sense aberrations common to the sample, whilst the aberrations experienced by light from the object of interest and the bead decorrelate with increasing separation, analogous to the ispolanatic patch in astronomical AO. The use of beads for AO has the drawback that one can only examine an object that happens to be located near a bead. There is a further disadvantage in that the beads cannot, in general, be injected into living samples. An alternative to beads is to generate an emitting source in the tissue by the use of a laser to generate scattering from the specimen, broadly analogous to using a laser guide star (LGS) in astronomical AO. The LGS approach allows the use of AO for arbitrary points in the tissue. Furthermore, long wavelength light in the red can be used for the LGS, negating the detrimental effects associated with fluorescent illumination. Typically, the laser light must be injected into the sample through the

MEMS Adaptive Optics VI, edited by Scot S. Olivier, Thomas G. Bifano, Joel Kubby, Proc. of SPIE Vol. 8253, 82530J · © 2012 SPIE · CCC code: 0277-786X/12/$18 · doi: 10.1117/12.909927

microscope objective, meaning that light scattered from other axial positions in the sample must be rejected. This has been done using either a confocal pinhole [9] or the short spatial coherence of a pulsed Ti:Sapphire laser [11]. However, there are a number of problems with using a laser probe – which we address in this paper. They are:

- The "double path effect" [12], whereby the system does not sense odd aberrations, must be corrected (and was ignored in refs [10] and [11].
- Null spot positions for the (Shack Hartmann) WFS must be defined accurately.
- Speckle noise in the WFS must be reduced.

In this paper we demonstrate a wide-field [13] AO corrected microscope, which uses techniques from ophthalmic AO to remove the double pass effect, and a vibrating mirror to reduce speckle. The system also uses wavefront sensorless AO to provide high quality nulls for the WFS, and to provide a reference to test the system.

2. MITTIGATING THE DOUBLE PASS EFFECT

2.1 Background

The double path effect occurs when a wavefront passes twice through the same aberrated medium in opposing directions. The result is that the odd coefficient aberrations varying with aperture such as coma, trefoil etc are canceled and thus the WFS is unable to sense them. This has been widely analyzed for ophthalmic AO [12,14]. One solution is to use a small diameter laser probe which only passes through a small part of the pupil, but after scattering passes through the full pupil on the return pass [15]. In addition, the incoming beam is also subjected to direct reflection on the cornea, which generates an extra set of intense spots on the WFS camera. In the case of ophthalmic AO a solution is to use an off-axis beam. In a microscope, the problem is similar as part of the incoming probe beam is reflected from the various surfaces normal to optical axis such as the cover slip and specimen interfaces.

2.2 Polarization used to reject reflected light

We demonstrate a method using the change in light polarization during the scattering process to discriminate the light coming from specular (direct reflection) and diffuse reflection (elastic scattering). It has been shown in [16], that light becomes depolarized as it travels deeply through tissue. Although such a characteristic has not been observed in scattered light by the retinal surface [14,17], it has been experimentally shown using polystyrene microspheres and biological tissues that the process increases with the optical depth. By using a polarization beam splitter just before the back aperture of the microscope objective, the incoming linear polarized light is reflected whilst half the out coming non polarized light generated by the diffuse reflection is transmitted to the WFS.

3. OPTICAL CONFIGURATION

The optical set-up is shown in Fig. 1(a). The sample is a 4-5 microns thick mouse back skin tissue (C57bl6/CBA F1 mice) stained with Hematoxylin and Eosin. The sample is illuminated from behind by a blue LED (emission peak at 470nm) and the light is collected by a Nikon Fluor (X100, NA 1.30) objective. We use a liquid light guide to carry the light from the LED to the sample to maximize the etendue. However, the illumination NA is less than the microscope objective collection NA and is estimated to be 0.84. Epi-illumination was not used due to the slight complication of the laser probe coupling but could be incorporated in future designs. The back aperture of the microscope (~6 mm) is re-imaged through a telecentric configuration composed of 2 lenses (f1 = 200 mm and f2 = 400 mm) onto the deformable mirror (DM), which is an Imagine Optics Mirao 52-e. After the DM, a beam-splitter sends the light into the first arm with a Thorlabs WFS via two lenses (f3 = 400 mm and f4 = 75 mm) working in a telecentric arrangement and a second arm composed of the science camera (Q-imaging Retiga 1300) at the focus of a lens (f5 = 200 mm). A confocal pinhole was placed between f3 and f4 to filter light scattered by tissue located away from the focal plan of the microscope objective. This pinhole is a variable diaphragm whose minimum size is 850 microns. The maximum amplitudes of Zernike modes that are not filtered by the pinhole are shown in Table 1. They vary from 0.37 waves RMS for spherical

aberration to 2.06 waves for astigmatism. This corresponds to a range of 5 to 30 times the diffraction limit based on the Maréchal criterion (0.07 waves RMS).

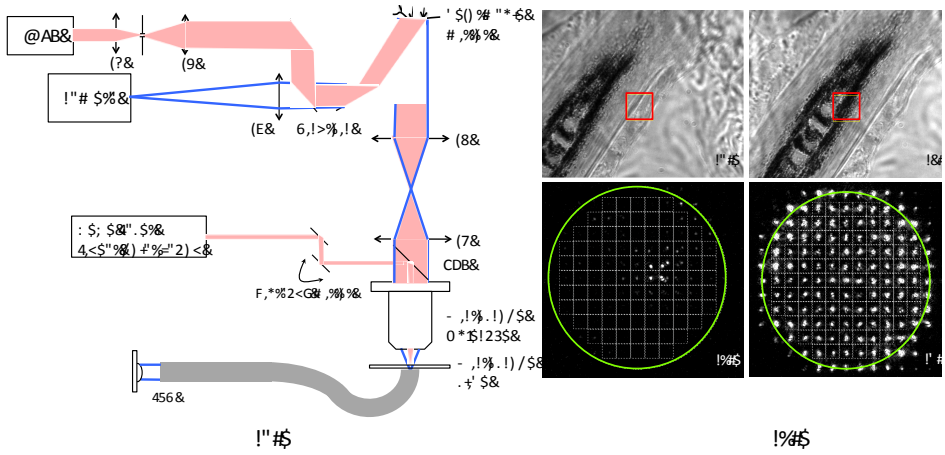

Fig. 1: (a) Closed loop adaptive optics microscope optical configuration. (b) The red box represents the location where the artificial guide star is generated. It is not visible as the laser wavelength has been filtered with a dichroic filter. The green circle corresponds to the microscope aperture. On Fig. (b-1), the artificial beacon has been placed on a low scattering area of the sample, which correspond to transparent tissues. Fig. (b-2) shows the WFS signal for Fig. (b-1). On Fig. (b-3), the laser is focusing onto a high scattering part of the tissue; the scattered light is covering the whole pupil Fig. (b-4).

The depth of field in the microscope objective focal plane for this pinhole size is equivalent to 3 micron sections, which is small enough to filter the specular reflection on both sides of the 0.17 mm cover slip.

The HeNe laser probe (633 nm, 2 mm in diameter) is injected just before the objective via reflection from a polarization beam splitter with the depolarized scattered light being transmitted by the beam-splitter. The scattered light is collected over the full NA of the microscope objective. As the probe laser is highly coherent, a speckle pattern appears at the WFS camera, which produces errors in the Shack Hartmann measurement and subsequent wavefront reconstruction. Here we used a similar technique to the one described in [11], where the speckle was averaged through different focal positions. In our case, we transversally scanned the probe beam at a much higher frequency (120Hz) than the frame rate of the WFS camera (10Hz). The Fig. 1-b shows the effect of diffuse reflection and specular reflection on a sample observed with our widefield microscope, in the WFS plan.

Table 1: Maximal Zernike mode amplitude transmitted by our 850 microns pinhole. Units are waves (λ = 633 nm).

Zernike Mode	Type	M – Maximal wave amplitude (RMS)
Z_1	Piston	-
Z_2 & Z_3	Tip & tilt	5.03
Z_4	Focus	1.46
Z_5 & Z_6	Astigmatism	2.06
Z_7 & Z_8	Coma	0.53
Z_9	Spherical aberration	0.37
Z_{10} & Z_{11}	Trefoil	1.17

4. EXPERIMENTAL DESCRIPTION AND RESULTS

A reference wavefront from a separate source can be used to provide a null reference position for the WFS spots, but this is prone to non-common path errors [18]. Instead we used a wavefront sensorless configuration to define the null position and then compared sensored and sensorless operation. We controlled the DM using a simplex optimization algorithm with an edge detection maximization as the metric. We then recorded a reference wavefront, from the back-scattered HeNe light, to define the reference spot locations on the Shack Hartmann WFS for the closed loop system. The sample was a black melanin spot in a mouse back skin hair follicle, in the red box in Fig. 2(a). (Later referred as sample 1).

With the WFS spots recorded for this optimized configuration the loop was then closed with the WFS now determining the correction to be placed on the mirror aiming for the recorded optimized wavefront. The stability of the loop is then checked by sending random aberrations composed of a set of low order Zernike modes to the DM to perturb the system. Focus was intentionally added to the random aberration. For each step, the RMS wavefront is recorded as well as the metric value. Fig. 2(b) – top, shows the variation of the RMS wavefront for 3 perturbations when the closed loop is enabled and the bottom chart shows the metric variation during the loop. For each perturbation, the system restores the minimum wavefront error and the maximum metric value within around 5 iterations.

With the stability of the loop confirmed we then opened the loop and another melanin spot (later referred to as sample 2) was placed in the region of interest (top / green box on Fig. 2(b)) and the laser probe was focused to the same area. The closed loop was then re-activated on sample 2 but using the reference wavefront recorded from sample 1. Fig. 3(a) shows the wavefront RMS error (top chart) and the image sharpness value (bottom chart) quickly converging to their optimal values. (As the melanin spot used for sample 2 is different than the one used for the calibration and the test, the absolute metric value between Fig 2(b) and 3(a) cannot be directly compared.) Thus we demonstrate that we can move, and subsequently observe, any arbitrary part of the object and remove resulting the aberrations using the original wavefront measurement as the target for the closed loop.

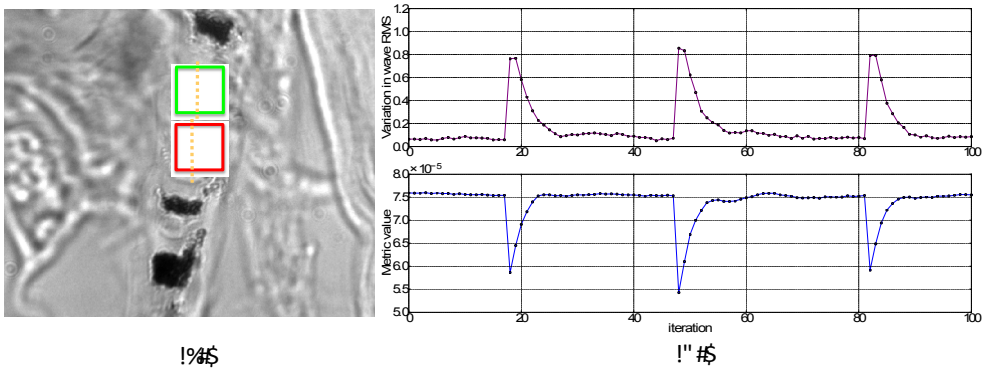

!%#$!" #$

Fig. 2: (a), Melanin dots in a hair follicle in back mouse tissue, on which the optimization and closed loop are run. The bottom (red) square corresponds to the sample one and the green (top) square is the sample 2 .The reference wavefront is recorded on the optimized image of the sample 1. (b) Recorded variation on the RMS wavefront (top - red) and metric value (bottom – blue) while the closed-loop is on for he sample 1, and when 3 perturbations are sent to the mirror

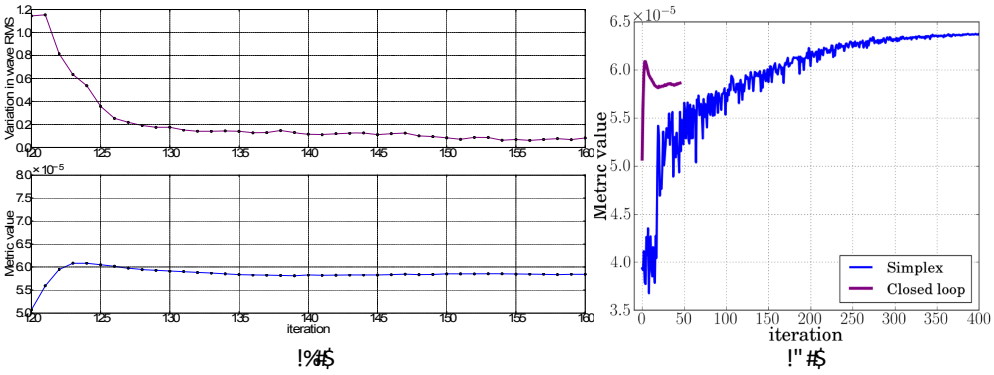

Fig. 3: On (a), RMS wavefront error (top) and metric value (bottom) when the closed loop is enabled on sample 2 using the reference wavefront recorded on sample 1. On (b), metric value comparison while the system is optimizing on sample 2 in a sensorless configuration using the simplex (in blue), and in a wavefront sensor based configuration (in violet). After reaching the plateau, in the closed loop configuration, the stability of the system is checked by sending random aberration onto the mirror.

5. CONCLUSIONS

We have demonstrated the use of partial confocal back scattered light from the sample as a reference source for a WFS in a closed loop AO microscope. We have implemented a design, which removes the double path effect as well as the reflection from the slide, and lens surface, which would otherwise confuse the WFS by adding extra sets of spots. We have demonstrated that the closed loop using the WFS is auto optimizing for different parts of the sample, using a common reference wavefront, but in this case, the accuracy of the loop is limited by the contribution of the spot shape to the center of mass measurement.he optimization using image sharpness metric gives slightly better results but takes significantly longer. We thus believe that both true closed loop AO and metric based optimization have a role to play in AO in microscopy.

ACKNOWLEDGEMENTS

The authors wish to acknowledge funding from the British Heart Foundation, in particular a Research Excellence Award, and the Engineering and Physical Science Research Council. All samples were used in accordance with UK Home Office rules. The sample (murine dorsal tissue incorporating with GFP expressing skin stem cells) has been supplied by Dr Carrie Ambler and Dr Richie Wong (Durham University).

REFERENCES

[1] J. M. Girkin, S. Poland, and A. J. Wright, “Adaptive optics for deeper imaging of biological samples,” Current Opinion in Biotechnology, vol. 20, no. 1, pp. 106 – 110, 2009.

[2] M. Booth, M. Neil, and T. Wilson, “Aberration correction for confocal imaging in refractive-index- mismatched media,” Journal of Microscopy, vol. 192, no. 2, pp. 90–98, 1998.

[3] M. Booth, “Wave front sensor-less adaptive optics: a model-based approach using sphere packings,” Opt. Express, vol. 14, pp. 1339–1352, Feb 2006.

[4] N. Olivier, D. Debarre, and E. Beaurepaire, “Dynamic aberration correction for multiharmonic microscopy,” Opt. Lett., vol. 34, no. 20, pp. 3145–3147, 2009.

[5] L. Sherman, J. Y. Ye, O. Albert, and T. B. Norris, "Adaptive correction of depth-induced aberrations in multiphoton scanning microscopy using a deformable mirror," Journal of Microscopy, vol. 206, no. 1, pp. 65–71, 2002.
[6] Sanford, K. K., Parshad, R. and Gantt, R. [Free Radicals, Aging, and Degenerative Diseases], Wiley-Liss, Inc, New York, 373-394 (1986)
[7] O. Azucena, J. Crest, S. Kotadia, W. Sullivan, X. Tao, M. Reinig, D. Gavel, S. Olivier, and J. Kubby, "Adaptive optics wide-field microscopy using direct wavefront sensing," Opt. Lett., vol. 36, pp. 825–827, Mar 2011.
[8] P. Vermeulen, E. Muro, T. Pons, V. Loriette, and A. Fragola, "Adaptive optics for fluorescence wide-field microscopy using spectrally independent guide star and markers," vol. 16, no. 7, p. 076019, 2011.
[9] X. Tao, B. Fernandez, O. Azucena, M. Fu, D. Garcia, Y. Zuo, D. C. Chen, and J. Kubby, "Adaptive optics confocal microscopy using direct wavefront sensing," Opt. Lett., vol. 36, pp. 1062–1064, Apr 2011.
[10] J. W. Cha and P. T. So, "A shack-hartmann wavefront sensor based adaptive optics system for multi- photon microscopy," in Biomedical Optics, p. BMD52, Optical Society of America, 2008.
[11] M. Rueckel, J. A. Mack-Bucher, and W. Denk, "Adaptive wavefront correction in two-photon microscopy using coherence-gated wavefront sensing," Proceedings of the National Academy of Sciences, vol. 103, no. 46, pp. 17137–17142, 2006.
[12] P. Artal, S. Marcos, R. Navarro, and D. R. Williams, "Odd aberrations and double-pass measurements of retinal image quality," J. Opt. Soc. Am. A, vol. 12, pp. 195–201, Feb 1995.
[13] It should be noted that we use the term "widefield" as defined in the microscopy community, meaning a non-beam scanned technique as opposed to widefield as defined by the AO community, which means a technique for correcting for multiple heights (or depths) of atmospheric turbulence.
[14] L. Diaz-Santana and J. C. Dainty, "Effects of retinal scattering in the ocular double-pass process," J. Opt. Soc. Am. A, vol. 18, pp. 1437–1444, Jul 2001.
[15] J. Liang, B. Grimm, S. Goelz, and J. F. Bille, "Objective measurement of wave aberrations of the human eye with the use of a hartmann-shack wave-front sensor," J. Opt. Soc. Am. A, vol. 11, pp. 1949– 1957, Jul 1994.
[16] S. L. Jacques, J. R. Roman, and K. Lee, "Imaging superficial tissues with polarized light," Lasers in Surgery and Medicine, vol. 26, no. 2, pp. 119–129, 2000.
[17] G. V. Blokland and D. V. Norren, "Intensity and polarization of light scattered at small angles from the human fovea," Vision Research, vol. 26, no. 3, pp. 485 – 494, 1986.
[18] Nathan P. Doble, Gordon D. Love, David F. Buscher, Richard M. Myers, and Alan Purvis, "The use of image quality metrics for correction of non-common path errors in the ELECTRA adaptive optics system". Proc. SPIE Vol. 3749,785-786 (1999)